


RESEARCH

Open Access



Effect of the mRNA decapping enzyme scavenger (DCPS) inhibitor RG3039 on glioblastoma

Hao Duan^{1†}, Yuan Xie^{1†}, Suwen Wu^{2†}, Guangyin Zhao^{3†}, Zhen Zeng⁴, Hongrong Hu¹, Yanjiao Yu¹, Wanming Hu⁵, Yuanzhong Yang⁵, Yukun Chen⁶, Haoqun Xie¹, Zexin Chen⁷, Gao Zhang⁸, Keith T. Flaherty⁹, Shanshan Hu¹⁰, Haineng Xu^{11*}, Wenjuan Ma^{12*} and Yonggao Mou^{1*} 

Abstract

Background Patients with glioblastoma (GBM) have a poor prognosis and limited treatment options. The mRNA decapping enzyme scavenger (DCPS) is a cap-hydrolyzing enzyme. The DCPS inhibitor RG3039 exhibited excellent central nervous system bioavailability in vivo and was safe and well tolerated in healthy volunteers in a phase 1 clinical trial. In this study, we investigated the expression of DCPS in GBM and the anti-tumor activity of RG3039 in various preclinical models of GBM.

Methods DCPS expression was examined in human GBM and paired peritumoral tissues. Its prognostic role was evaluated together with clinicopathological characteristics of patients. The anti-GBM effect of RG3039 was determined using GBM cell lines, patient-derived organoids, and orthotopic mouse models. The therapeutic mechanisms of DCPS inhibition were explored.

Results DCPS is overexpressed in GBM and is associated with poor survival of patients with GBM. The DCPS inhibitor RG3039 exhibited robust anti-GBM activities in GBM cell lines, patient-derived organoids and orthotopic mouse models, with drug exposure achievable in humans. Mechanistically, RG3039 downregulated STAT5B expression, thereby suppressing proliferation, survival and colony formation of GBM cells.

Conclusions DCPS is a promising target for GBM. Inhibition of DCPS with RG3039 at doses achievable in humans downregulates STAT5B expression and reduces proliferation, survival and colony formation of GBM cells. Given the excellent anti-cancer activity and central nervous system bioavailability in vivo and good tolerance in humans, RG3039 warrants further study as a potential GBM therapy.

[†]Hao Duan, Yuan Xie, Suwen Wu and Guangyin Zhao contributed equally to this work.

*Correspondence:

Haineng Xu
haineng@pennmedicine.upenn.edu
Wenjuan Ma
mawenj@sysucc.org.cn
Yonggao Mou
mouyg@sysucc.org.cn

Full list of author information is available at the end of the article



© The Author(s) 2024. **Open Access** This article is licensed under a Creative Commons Attribution-NonCommercial-NoDerivatives 4.0 International License, which permits any non-commercial use, sharing, distribution and reproduction in any medium or format, as long as you give appropriate credit to the original author(s) and the source, provide a link to the Creative Commons licence, and indicate if you modified the licensed material. You do not have permission under this licence to share adapted material derived from this article or parts of it. The images or other third party material in this article are included in the article's Creative Commons licence, unless indicated otherwise in a credit line to the material. If material is not included in the article's Creative Commons licence and your intended use is not permitted by statutory regulation or exceeds the permitted use, you will need to obtain permission directly from the copyright holder. To view a copy of this licence, visit <http://creativecommons.org/licenses/by-nc-nd/4.0/>.

Keywords Glioblastoma, DCPS, RG3039, STAT5B

Background

Glioblastoma (GBM) is the primary malignant tumor of the central nervous system (CNS) with the highest morbidity and mortality among all malignant CNS tumors [1]. The standard treatment for GBM is surgical resection combined with Stupp regimen and tumor-treating fields. Despite the availability of treatment, the prognosis of GBM remains dismal, with a median overall survival (OS) less than 2 years [2]. Therefore, the development of new, effective treatments is critical.

The vigorous biological activities of tumor cells require large amounts of mRNAs. After translation, mRNAs are degraded to maintain steady-state levels, a critical determinant in the regulation of gene expression [3]. Decapping, the cleavage of the 5' cap structure, is an essential step in mRNA degradation. Cap degradation intermediates recruit and bind cap-binding proteins [4], which regulate subsequent processes, including nuclear mRNA processing, nuclear export, and translation [4, 5]. The mRNA decapping enzyme scavenger (DCPS) is a cap-binding enzyme that performs hydrolyzing the cap degradation intermediates at the final step [6, 7]. As its activity influences the amount of cap degradation intermediates, thereby influencing the function of cap-binding proteins, DCPS regulates the steady-state levels of mRNA.

The DCPS inhibitor RG3039, an orally active quinazoline derivative, was originally discovered in a high-throughput drug screen for the treatment of spinal muscular atrophy (SMA). In pre-clinical studies, RG3039 robustly inhibited DCPS enzyme activity and showed excellent CNS bioavailability *in vivo* [8, 9]. A phase 1 clinical trial of RG3039 showed that RG3039 was safe and well tolerated at the highest dose tested (3 mg/kg) in healthy volunteers. Yamauchi et al. performed genome-wide CRISPR-Cas9 screening *in vitro* and *in vivo* and found that DCPS was required in acute myeloid leukemia (AML) cells but was not essential for normal human hematopoietic cells [10]. RG3039 exhibited anti-leukemic effects *in vitro* and in AML patient-derived xenograft models *in vivo* [10].

In this study, we investigated the expression of DCPS in GBM, and the potential anti-GBM effect of the DCPS inhibitor RG3039. The expression of DCPS was significantly higher in GBM than in adjacent normal brain tissues, and higher expression of DCPS was associated with poorer prognosis. Results using patient-derived GBM organoids (GBOs) and orthotopic GBM mouse models indicate that RG3039 may be a safe and effective anti-GBM agent with drug exposures achievable in humans.

Materials and methods

Ethical statement, sample and clinical data collection

The Medical Ethics Committee of Sun Yat-sen University Cancer Centre approved this study (no. B2020-165-01 and B2021-427-01). All procedures involving human participants were performed in accordance with the ethical standards of the Medical Ethics Committee of Sun Yat-sen University Cancer Centre and followed the 1964 Helsinki Declaration and its later amendments.

Fresh surgically resected tumor tissues and their paired peritumoral tissues were obtained from 28 patients with newly diagnosed GBM at the Sun Yat-sen University Cancer Center between July 2020 and June 2022. Frozen sections were made and reviewed by an experienced pathologist immediately after surgical resection to confirm a preliminary diagnosis of high-grade glioma without necrosis and an absence of tumor in peritumoral tissues. Fresh tumor tissues were sectioned into two parts; one was placed in sterile PBS for organoid culture, and the other sample, along with peritumoral tissues, was snap-frozen in liquid nitrogen and stored at 80 °C for protein or genomic DNA extraction. Whole blood samples (2 mL) of patients were obtained preoperatively and stored at 80 °C for subsequent genomic DNA extraction.

Medical records and archived formalin-fixed, paraffin-embedded (FFPE) tissues of 62 patients who were newly diagnosed with GBM and underwent surgical resection at Sun Yat-Sen University Cancer Center between January 2013 and December 2016 were retrospectively retrieved. Clinicopathological data including patient age at diagnosis, sex, location of tumors, tumor numbers, tumor size, preoperative Karnofsky performance status (KPS), subventricular zone (SVZ) involvement described by Lim et al. [11], extent of resection (EOR), adjuvant therapy, isocitrate dehydrogenase 1 (IDH-1) mutation status, and O6-DNA-methylguanine methyltransferase (MGMT) promoter methylation status were collected from medical records. The EOR was qualitatively determined by the residual enhancing tumor in T1-enhanced scans of postoperative magnetic resonance imaging (MRI). Gross total resection (GTR) was defined as the absence of residual enhancing tumor, and subtotal resection (STR) was defined as an enhancing tumor residue that constituted less than 50% of the sample. The last date of follow-up was December 2021. Survival status of patients was determined from clinical attendance records or direct telecommunication with patients or their families. OS was defined as the time between initial surgery and cancer-caused death or the date of last follow-up.

An experienced pathologist reviewed the hematoxylin-eosin (HE) staining of the surgically resected tumor

samples and selected the most representative GBM tissue of each patient and peritumoral normal brain tissues from five patients for further immunohistochemical analysis of DCPS expression.

Publicly available gene expression and survival data of patients in The Cancer Genome Atlas (TCGA) and Chinese Glioma Genome Atlas (CGGA) data sets were obtained from TCGA (<https://portal.gdc.cancer.gov>), GEPIA 2 (<http://gepia2.cancer-pku.cn>) and CGGA (<http://www.cgga.org.cn/>).

Cell culture and lentiviral transfection

Human GBM cell lines U87, U118, A172 and U251 were purchased from the Cell Bank of the Chinese Academy of Sciences (Shanghai, China). Cells were cultured in DMEM (C11995500BT, Gibco) supplemented with 10% FBS (10099141 C, Gibco) under standard culture conditions (5% CO₂, 37 °C). Normal human astrocytes HA1800 were purchased from ScienCell (Carlsbad, CA, USA) and cultured in Astrocyte Medium (1801; ScienCell).

To generate lentivirus, 293T cells were co-transfected with packaging vectors (LT003, Genecopoeia) and lentiviral expression vectors that express STAT5B and firefly luciferase for 8 h. After replacement with fresh medium and incubation for 48 h, medium supernatants containing lentivirus were collected. U87 and U251 cells were infected with lentivirus in the presence of 8 µg/ml polybrene (TR1003G, MilliporeSigma). Stable cell lines were selected with 2 µg/ml puromycin and maintained in medium with 1 µg/ml puromycin.

GBO culture and treatment

GBO culture was performed following previously published methods [12]. To measure the growth of GBOs, similarly sized GBOs (0.5–1 mm diameter) were placed into individual wells of a 48-well tissue culture plate with 300 mL of GBO medium containing 10 µM RG3039 (HY-102020, MedChemExpress) or solvent (DMSO) per well. GBO medium containing 10 µM RG3039 or solvent (DMSO) was replaced every 5 days. Images of individual GBOs were taken every 5 days using a brightfield microscope. The 2D projected area of each GBO was quantified in ImageJ by carefully outlining each GBO and measuring the area within the outlined region. The 2D area at each time point was divided by the 2D area at day 0 to calculate the growth ratio for each time point. Three individual GBOs were measured for each GBO sample.

For histological analysis, similarly sized GBOs (0.5–1 mm diameter) were placed into individual wells of a 48-well tissue culture plate with 300 mL of GBO medium containing specific concentrations of RG3039 or solvent (DMSO) per well. After 48 h, GBOs were fixed in formalin, embedded in paraffin, and subjected to H&E

and IHC staining. Three or four individual GBOs were measured for each GBO sample.

To measure the IC₅₀ of RG3039 and temozolomide (TMZ) on GBOs, GBOs were dissociated into smaller clusters containing approximately 2000 cells, resuspended in 36 µL culture medium, and seeded in each well of a 384-well plate. After 48 h, 4 µL of a threefold dilution series of each drug was dispensed separately, and three technical replicates of each drug were tested on three plates. After 3 days, cell viability was quantitated using the CellTiter-Glo 3D Cell Viability Assay (G9681, Promega) following the manufacturer's instructions. Relative luminescence units (RLU) for each well were normalized to the median RLU from the DMSO control wells, used as 100% viability. IC₅₀ values were generated using Prism 9 (GraphPad Software, Boston, MA, USA).

siRNA transfection

Cells were transfected with non-targeting control siRNA or siRNA targeting DCPS using Lipofectamine 3000 (L3000008, Invitrogen) in serum-free Opti-MEM medium (31985070, Gibco) for 12 h, followed by recovery with 10% FBS-supplemented DMEM for 24 h. DCPS siRNA was designed and synthesized by GenePharma (Shanghai, China): 5'-GCTCGATGACTTGTACTTGA T-3' (siDCPS).

Cell proliferation assay and half-maximal inhibitory concentration (IC₅₀) of RG3039

A CCK-8 assay (CK04-1000t, DOJINDO) was used to monitor cell viability. Briefly, cells were seeded into 96-well plates and cultured for specific times. The IC₅₀ of RG3039 was calculated using the OD₄₅₀ values at 72 h of culture.

Apoptosis assay

Cells were treated with various concentrations of RG3039 or solvent (DMSO) for 48 h. Apoptosis was evaluated using the APC Annexin V Apoptosis Detection Kit (640932, Biolegend) following the manufacturer's instructions.

Colony formation

Cells were seeded into 6-well plates at a density of 500 cells/well and treated with specific concentrations of RG3039 or solvent (DMSO) for 14 days. The culture media containing RG3039 or solvent was replaced once on day 7. After crystal violet staining, the visible colonies were counted.

Quantitative RT-PCR

Total RNA was extracted from treated cells using the MolPure[®] Cell RNA Kit (19231ES08, Yeasen) following the manufacturer's instructions. cDNA synthesis was

performed using the Hifair[®] III 1st Strand cDNA Synthesis Kit (11139ES10, Yeasen). PCR amplification was carried out in triplicate with Hieff UNICON[®] qPCR SYBR Green Master Mix (11199ES03, Yeasen) on a LightCycler[®] 480 System (Roche Diagnostics, Indianapolis, IN, USA). Primers were designed and synthesized by Angke Biotech (Guangzhou, China). Relative mRNA expression was evaluated by the $2^{-\Delta\Delta C_t}$ method and normalized to β -actin expression.

The sequences of the primers were as follows: STAT5B (FP: 5'-CAGAACACGTATGACCGCTG-3'; RP: 5'-CTG GAGAGCTACCATTGTTGG-3'), ATOH7 (FP: 5'-AAA GCTGTCCAAGTACGAGAC-3'; RP: 5'-CGAAGTGCT CACAGTGGAG-3'), DRNT1 (FP: 5'-CACCTAGACTC ATCACTTAGATCCACC-3'; RP: 5'-GAGACCTGATG GCTACAACCTGACA-3'), DRNT2 (FP: 5'-TGGAGAAG CGATGGATGACAGAGA-3'; RP: 5'-GGTGAACGGAC ACAATTGCCAGAA-3'), and ATCB (FP: 5'-CATGTAC GTTGCTATCCAGGC-3'; RP: 5'-CTCCTTAATGTCAC GCACGAT-3').

Western blot analysis

Protein extraction was performed with RIPA buffer (89900, Thermo Scientific) containing the Protease and Phosphatase Inhibitor Cocktail (78441, Thermo Scientific). The samples were electrophoresed by SDS-PAGE and transferred to PVDF membranes. The membranes were blotted with antibodies against GAPDH (1:5000, 5174 S, CST), DCPS (1:1000, MA5-26131, Invitrogen), or STAT5B (1:1000, 34662 S, CST) at 4 °C overnight. Protein bands were detected with secondary antibodies specific for mouse or rabbit IgG (1:5000, SA00001-1 or SA00001-2, Proteintech), followed by ECL (WBKLS0100, MilliporeSigma) development.

Immunohistochemistry (IHC) staining and analysis

FFPE sections were de-paraffinized, rehydrated, and treated with 3% H₂O₂ at 37 °C for 10 min. The sections were subjected to antigen retrieval in antigen retrieval buffer (HK086-9 K Biogenex) at 95 °C for 20 min. After blocking non-specific antigens with 5% horse serum for 1 h at room temperature, the sections were incubated with antibodies against DCPS (1:100, MA5-26131, Invitrogen), Ki-67 (1:500, ZM-0167-0.2, ZSGB-BIO), GFAP (1:500, ZA-0529-0.2, ZSGB-BIO) or Olig-2 (1:10, ZA-0561-1.5, ZSGB-BIO) overnight at 4 °C, followed by incubation with secondary antibody at room temperature for 30 min. The slides were washed in PBS and stained with 3,3-diaminobenzidine (DAB). Finally, the sections were counterstained using Mayer's hematoxylin, dehydrated and mounted. The average percentage of positive cells under five high-power fields (HPFs) was recorded as the final expression score for each section.

DCPS expression was scored using previously described methods [13, 14]. The intensity (I) and proportion (Prop) of staining in each section were recorded; I is the intensity of staining (defined as no=0, weak=1, moderate=2, and strong=3) and Prop is the fraction of positive cells, expressed as a percentage (0–100%). Scores were calculated as follows: score=I × Prop. The final DCPS expression score of each patient was calculated as the average score under three HPFs. The median DCPS expression score of all patients was defined as the cut-off point for high and low expression.

Whole exome sequencing (WES)

Genomic DNA was extracted from pieces of parental tumors (at least 0.5 cm diameter) or organoids at 2 weeks and a 0.5 mL aliquot of whole blood with the DNeasy Blood and Tissue Kit (69506, Qiagen). DNA quality was assessed using a Nano-drop 2000 (Thermo Fisher Scientific, Waltham, MA, USA) and quantified using the Qubit 4.0 Fluorometer (Thermo Fisher Scientific). Libraries were constructed with SureSelect Human All Exon V6 (Agilent Technologies, Santa Clara, CA, USA) and subjected to deep sequencing (150 PE, approximately 80 megabyte reads for each sample, Illumina NovaSeq 6000) at HaploX (Shenzhen, Guangdong, China). Raw Fastq reads were trimmed with Trimmomatic (v0.36) as previously described [15] and then aligned in paired-end mode to the hg19 reference genome using BWA-MEM with default parameters to generate a binary sequence alignment map file [16]. Data preprocessing was performed by the Genome Analysis ToolKit (v4.1.1.0) following the best practice guidelines [17, 18]. Somatic single nucleotide variants (SNVs) were detected using MuTect (v1.1.7) [19]. Annotator (v2022-03-20) was used to annotate the result to detect somatic copy number variations (CNVs).

RNA sequencing (RNAseq)

Cells (2×10^6) were treated with RG3039 (6 μM) or vehicle (DMSO) for 48 h, lysed in 1 ml TRIzol (15-596-018, Invitrogen) and subjected to RNA extraction using the MolPure[®] Cell/Tissue Total RNA Kit (19221ES50, Yeasen) following the manufacturer's instructions; RNA was purified with an RNeasy Plus Mini Kit (74136, Qiagen). After a quality control step with the RNA Nano 6000 Assay Kit of the Bioanalyzer 2100 system (Agilent Technologies), libraries were constructed with the NEBNext[®] UltraTM RNA Library Prep Kit for Illumina[®] (E7530L, NEB) and subjected to deep sequencing (150 PE, approximately 60 megabyte reads for each sample, Illumina NovaSeq 6000) at Novogene (Beijing, China). The sequences were aligned to the UCSC hg38 reference genome using RNA-STAR (v2.4.2a). Gene expression was normalized and calculated as fragments per kilobase million (FPKM) values by Cufflinks (v2.2.1) with Gencode v22 gene annotations.

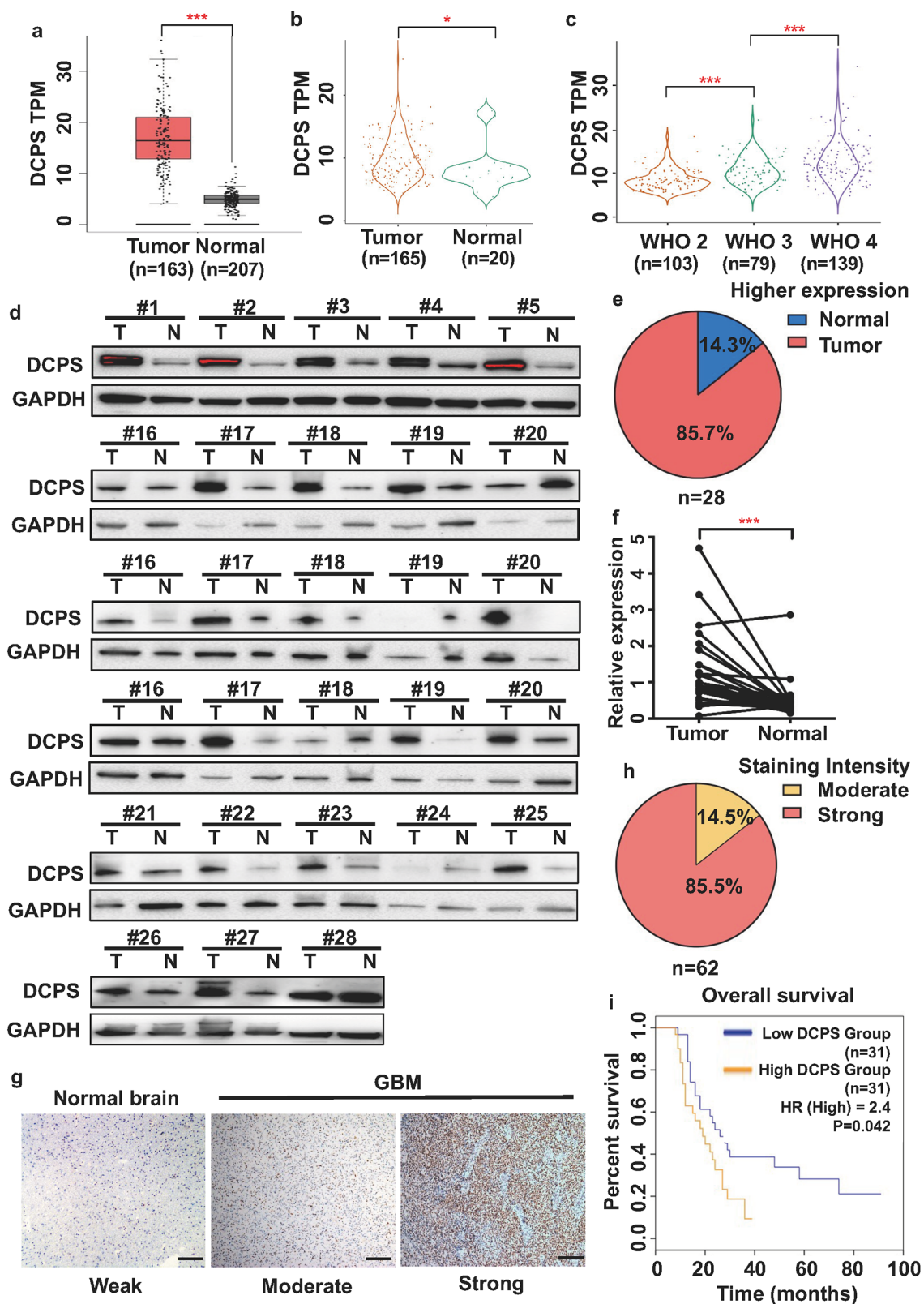


Fig. 1 (See legend on next page.)

(See figure on previous page.)

Fig. 1 DCPS expression was elevated in GBM and associated with poor survival of GBM patients

(a) The expression of DCPS in GBMs ($n=163$) and normal brain tissues ($n=207$) in TCGA database. Statistical analysis by Wilcoxon test, $***, p < 0.001$

(b) The expression of DCPS in GBM ($n=165$) and normal brain tissue ($n=20$) in the CGGA database. Statistical analysis by Wilcoxon test, $*, p < 0.05$

(c) The expression of DCPS in various grades of glioma ($n=103$ for WHO grade 2; $n=79$ for WHO grade 3; $n=139$ for WHO grade 4) in the CGGA database. Statistical analysis by Kruskal–Wallis test, $***, p < 0.001$

(d) Western blot analysis of DCPS expression in paired tumor and normal brain tissues from patients with GBM ($n=28$)

(e–f) Quantified data of western blot of DCPS expression in paired tumor and normal brain tissues from patients with GBM ($n=28$). (e) DCPS expression was elevated in tumor tissues compared with the paired normal brain tissues in 85.7% of GBM patients. (f) DCPS protein expression in tumor tissues was significantly higher than that in the paired normal brain tissues. Statistical analysis by paired t-test, $***, p < 0.001$

(g–h) IHC staining of DCPS expression in GBMs ($n=62$) and normal brain tissues ($n=5$). Scale bar, 150 μm . (g) Representative images. (h) Quantification of IHC staining intensity of DCPS in GBMs ($n=62$)

(i) Correlation of DCPS expression with overall survival was analyzed in patients ($n=62$) from our hospital. Statistical analysis by two-sided log-rank test

Orthotopic GBM mouse model and treatment

BALB/c nude mice (6 weeks old) were obtained from Shanghai Model Organisms (Shanghai, China). Mice were bred, housed in sterilized isolated cages, maintained under a 14-h light/10-h dark cycle, and provided sterilized food and water ad libitum in the experimental animal center of Sun Yat-sen University Cancer Centre. The Experimental Animal Ethics Committee of Sun Yat-sen University Cancer Centre approved the animal experiments. An orthotopic GBM model was induced in mice, as described previously [20]. Briefly, mice were anesthetized and placed onto a stereotactic frame (Stoelting, Wood Dale, IL, USA). After making a 1-cm parasagittal incision on the skin and a 1-mm burr hole on the skull, 2 μL PBS containing 2×10^5 U87-luc or U251-luc cells was injected 2 mm deeply into the parenchyma at 2 mm lateral and 2 mm posterior to the anatomic bregma over the right hemisphere. Tumor growth was detected by whole-body bioluminescence. Tumor-bearing mice were randomized to receive treatment, and the investigators were not blinded. Mice were treated with intraperitoneal (i.p.) injections with TMZ (20 mg/kg) for 5 days or RG3039 (20 mg/kg) or vehicle (water) once a day until the endpoint of observation. The endpoint of observation was defined as occurrence of a crouched body or weight loss to 16 g.

In vivo bioluminescence imaging

One week after tumor cell injection, in vivo bioluminescence was performed to track the growth of engrafted tumor cells every 3 to 4 days until the endpoint of observation. Mice were anesthetized and retro-orbitally injected with luciferin (150 mg/kg, 122799, PerkinElmer, Waltham, MA, USA). Images measuring the bioluminescent activity of the luciferase enzyme were acquired using the IVIS Lumina II Spectrum Imaging System (Caliper Life Sciences, Hopkinton, MA, USA). Fixed-area regions of interest (ROIs) were created, and photons emitted from the ROIs were quantified by $\text{P s}^{-1} \text{cm}^{-2} \text{sr}^{-1}$ using Living Image software (Caliper Life Sciences).

Statistics

The Prism 9 (GraphPad, San Diego, CA, USA) and SPSS 22 (IBM, Armonk, NY, USA) software were used for statistical analyses. OS of patients was defined as the time between initial surgery and tumor-caused death or the date of last follow-up. Univariate survival analyses were performed by the Kaplan–Meier method, and the differences were assessed using the log-rank test. The Cox proportional hazards model was used for the multivariate survival analysis. The independent Student's t test, Wilcoxon test, and Kruskal–Wallis test were used to assess the statistical significances between two groups. A two-sided P value < 0.05 was considered statistically significant.

Results

DCPS expression was elevated in GBM and associated with poor survival of GBM patients

We first surveyed TCGA data and assessed DCPS expression in tumor and normal tissues in various malignancies. The expression of DCPS in tumor tissues was higher than in normal tissues in most types of malignancies. The differences were particularly pronounced in diffuse large B-cell lymphoma, GBM, kidney chromophobe, lower grade glioma, pancreatic adenocarcinoma, skin cutaneous melanoma, stomach adenocarcinoma, and thymoma (Figure S1a).

We further investigated the expression of DCPS in GBM. Analysis of RNA sequencing (RNAseq) data of TCGA GBM specimens in comparison with controls showed that DCPS expression was significantly higher in GBM tissues ($n=163$) than in normal brain tissues ($n=207$) (unpaired t-test, $p < 0.001$) (Fig. 1a). Similar results were obtained in the CGGA for Chinese patients with GBM (unpaired t-test, $p < 0.05$) (Fig. 1b). Analysis of the CGGA glioma tissues demonstrated a significantly higher expression level of DCPS in higher-grade glioma (unpaired t-test, $p < 0.001$) compared with lower-grade glioma (Fig. 1c). To substantiate our results, we next assessed DCPS expression in paired tumor and normal brain tissues from 28 patients with GBM using western blot analysis (Fig. 1d). Patients with higher DCPS

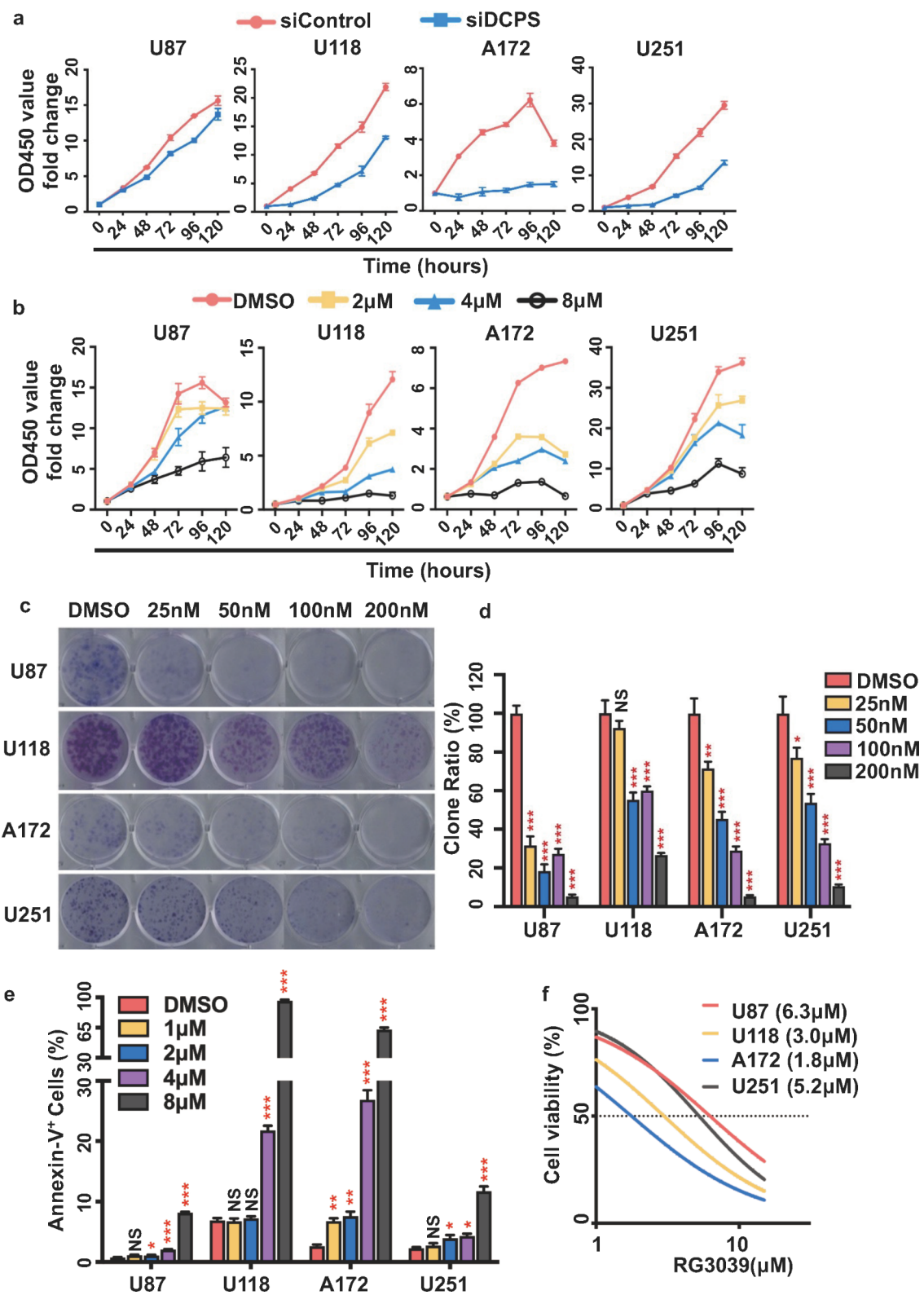


Fig. 2 (See legend on next page.)

(See figure on previous page.)

Fig. 2 Targeting DCPS suppressed proliferation and colony formation and induced apoptosis of GBM cells

(a) GBM cell lines were transfected with siRNA targeting DCPS. Cell proliferation was monitored by CCK-8 assay for 120 h. Quantification of the fold change of the OD450 value at each time point compared with that at 0 h (mean \pm SEM, $n=3$)

(b) GBM cell lines were treated with various concentrations of RG3039 or DMSO. Cell proliferation was monitored by CCK-8 assay for 120 h. Quantification of the fold change of the OD450 value at each time point compared with that at 0 h (mean \pm SEM, $n=3$)

(c) Representative images of colony formation of GBM cell lines treated with various concentrations of RG3039 or DMSO for 14 days

(d) Quantification of the ratio of colony formation of GBM cells treated with RG3039 to that of cells treated with DMSO (mean \pm SEM, $n=3$). Statistical analysis by unpaired t-test, NS, no significance, *, $p < 0.05$, **, $p < 0.01$, ***, $p < 0.001$

(e) Quantified data of Annexin-V-positive cells in apoptosis assays (see Figure S2a for details) in GBM cell lines treated with specific concentrations of RG3039 or DMSO (mean \pm SEM, $n=3$). Statistical analysis by unpaired t-test, NS, no significance, *, $p < 0.05$, **, $p < 0.01$, ***, $p < 0.001$

(f) GBM cell lines were treated with various concentrations of RG3039 or DMSO for 72 h. The IC₅₀ of RG3039 was analyzed by CCK-8 assay ($n=3$)

expression in tumor tissue than in paired normal brain tissue accounted for 85.7% of GBM patients (paired t-test, $p < 0.001$) (Fig. 1e-f). Consistent with the above results, IHC staining of 62 surgically resected GBM tissues showed that DCPS was strongly and moderately expressed in 85.5% and 14.5% of GBM samples, respectively, whereas normal brain tissue showed weak positive staining (Fig. 1g-h).

We next examined the association of DCPS expression with the survival of patients with GBM in TCGA datasets and our own patient cohort. In the TCGA GBM cohort, patients with a higher DCPS expression in tumors had a significantly shorter OS than those with lower DCPS expression (HR=1.5; log-rank test $p=0.039$; Figure S1b). The prognostic significance of DCPS expression was further confirmed by multivariate survival analysis in our patient cohort. In the Cox proportional hazards model, DCPS expression along with SVZ involvement, EOR and adjuvant therapy were independent prognostic factors for patients with GBM (Table S1). Patients with lower DCPS expression had a median OS of 26 months, whereas patients with higher DCPS expression had a significantly shorter median OS of 19 months (HR=2.4; log-rank test $p=0.042$; Fig. 1i, Table S1).

Taken together, our data indicated that DCPS expression was elevated in GBM, and was associated with poor survival of GBM patients.

Targeting DCPS suppressed proliferation and colony formation and induced apoptosis of GBM cells

We next investigated the tumor-promoting effects of DCPS in vitro. First, we detected the expression of DCPS in four human GBM cell lines: U87, U118, A172 and U251 (Figure S1c). We knocked down the expression of DCPS in GBM cell lines by siRNA, and decreased expression was confirmed by western blotting (Figure S1d). Proliferation assays showed that interference of DCPS expression impeded the proliferation of tumor cells (Fig. 2a). We next treated GBM cell lines with the DCPS inhibitor RG3039. RG3039 efficiently suppressed the proliferation and colony formation of tumor cells in a concentration-dependent manner (Fig. 2b-d). Furthermore, RG3039 significantly induced apoptosis of tumor

cells (Fig. 2e & S2a). The IC₅₀ of RG3039 on the GBM cell lines ranged from 1.8 μ M to 6.3 μ M (Fig. 2f). We also investigated the side effects of RG3039 on normal astrocytes. After treating normal human astrocytes with 8 μ M RG3039 for 48 h, less than 4% of the cells underwent apoptosis (Figure S2b, c). Taken together, these results demonstrated that inhibiting DCPS, either genetically or pharmacologically, suppressed the proliferation and colony formation activities of GBM cells and induced their apoptosis, while RG3039 exerted mild toxicity on normal astrocytes.

The anti-GBM activity of DCPS inhibitor RG3039 was comparable to that of TMZ

Traditional in vitro cell lines have limitations in reflecting the histology and mutational diversity of parental tumors. Therefore, we used GBOs that better recapitulated histological features and mutational profiles of parental tumors to assess the anti-GBM activity of RG3039.

To demonstrate the consistency between parental tumors and their corresponding GBOs, we performed HE and IHC staining with a panel of markers specific to GBM, including GFAP, Olig-2 and Ki-67. HE staining showed that both the GBO and the parental tumor had abundant cytoplasm, enlarged nuclei with noticeable atypia, and visible mitotic figures. IHC staining revealed that both the GBO and the parental tumor exhibited diffuse expression of GFAP and partial expression of Olig-2, while also having similar Ki-67 indexes. The results indicated that GBOs exhibited the same morphologic and histologic features as parental tumors (Figure S3a). We also performed WES on three pairs of GBOs and parental tumors to determine whether the GBOs maintained the genomic features of parental tumors. The somatic mutation profiles of GBOs were nearly identical to corresponding parental tumors. Both GBOs and parental tumors shared similar types of SNVs (Figure S3b). GBOs retained approximately 70–80% of SNVs that were identified in parental tumors (Figure S3c). Analysis of CNVs revealed that GBOs and their parental tumors shared similar regions of DNA loss and gain (Figure S3d).

To further clarify the anti-tumor activity of RG3039 toward GBOs, we treated GBOs from three cases with

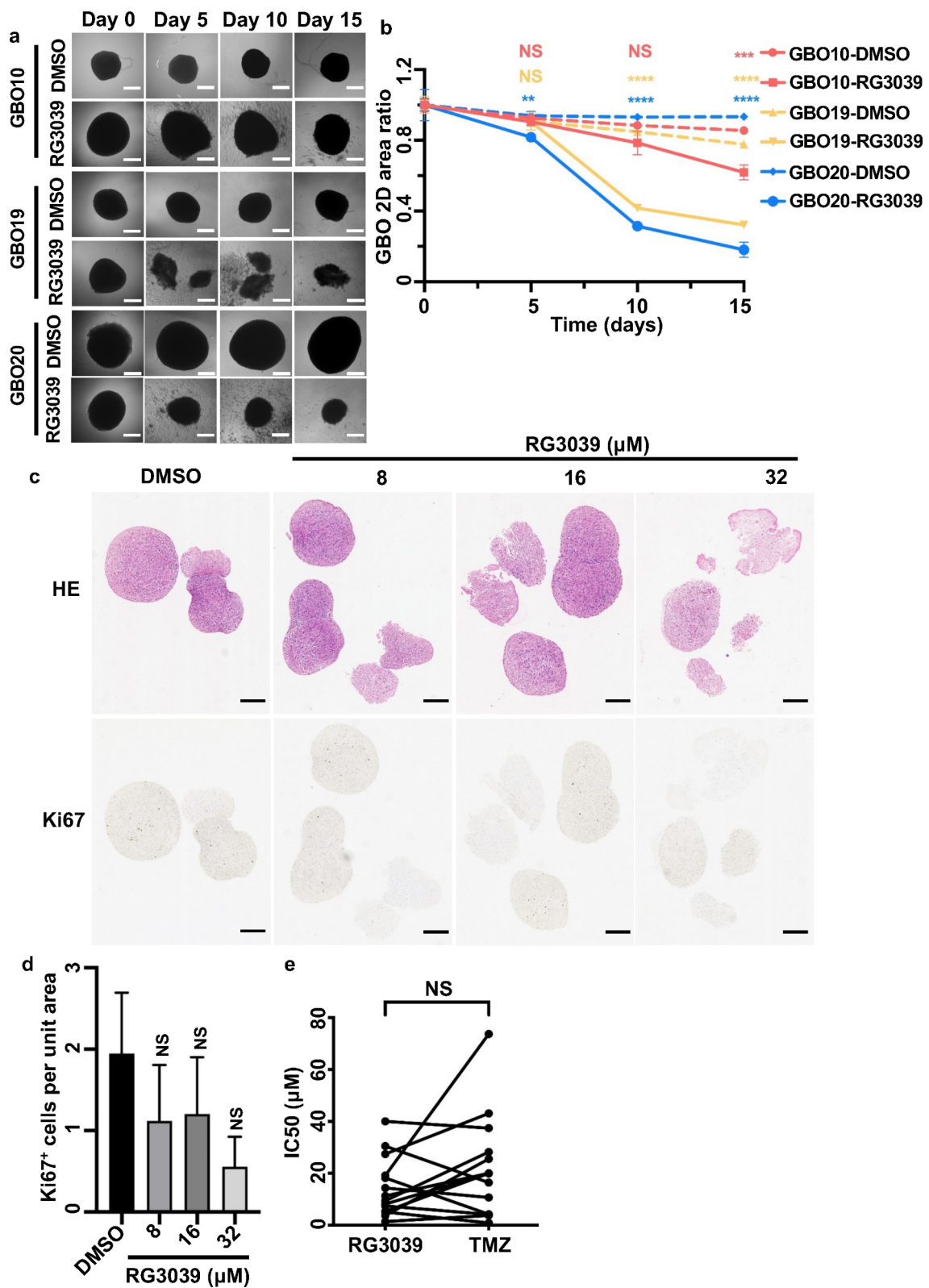


Fig. 3 (See legend on next page.)

(See figure on previous page.)

Fig. 3 The anti-GBM effects of RG3039 on patient-derived GBM organoids (GBOs)

(a–b) Growth of GBOs treated with RG3039 (10 μ M) or DMSO for 15 days (a) Representative bright-field images of GBOs. Scale bar, 250 μ m. (b) Quantification of the ratio of the 2D area at each time point to that at day 0 for the same GBOs (mean \pm SEM, $n=3$). Statistical analysis by unpaired t-test, NS, no significance, **, $p < 0.01$, ***, $p < 0.001$, ****, $p < 0.0001$

(c) Representative images of H&E staining and IHC staining for Ki67 of GBOs treated with RG3039 (8 μ M, 16 μ M, or 32 μ M) or DMSO for 48 h. Scale bar, 250 μ m

(d) Quantification of Ki67⁺ positive cell density in GBOs treated with RG3039 (8 μ M, 16 μ M, or 32 μ M) or DMSO in IHC staining (mean \pm SEM, $n=3$). Statistical analysis by unpaired t-test, NS, no significance

(e) Comparison of IC₅₀ of RG3039 and TMZ in GBOs ($n=14$). Statistical analysis by paired t-test, NS, no significance

RG3039 at a concentration of 10 μ M and measured the two-dimensional (2D) area of the GBOs. A 5-day treatment with RG3039 markedly inhibited the growth of GBOs, although the significance of inhibition varied among GBOs (Fig. 3a–b). Histological analysis revealed that RG3039 exhibited anti-GBM activities in a concentration-dependent manner. After 48 h of treatment with RG3039 at concentrations of 8 μ M, 16 μ M, or 32 μ M, the number of cells that stained positive for Ki67 in GBOs decreased as the RG3039 concentration increased (Fig. 3c–d). Additionally, the morphological structure of GBOs was disintegrated after the 48-h treatment with RG3039 at 32 μ M, which indicated complete death of GBOs (Fig. 3c).

TMZ is the first-line chemotherapeutic drug for GBM. Next, we further compared the IC₅₀ of RG3039 and TMZ on GBOs from 14 patients. The IC₅₀ of RG3039 was comparable to that of TMZ (Fig. 3e). These results indicated that the anti-GBM activity of RG3039 was equivalent to that of TMZ in vitro.

We next orthotopically transplanted human GBM cells (U251 or U87 cells) into brains of immunodeficient mice to assess the anti-GBM efficacy of RG3039 in vivo. The median OS of mice transplanted with U251 cells in the control group, TMZ group and RG3039 group were 23 days, 27 days and 29 days, respectively. Both TMZ and RG3039 significantly prolonged the survival of mice transplanted with U251 cells. The survival curves of the TMZ group and the RG3039 group were similar (Fig. 4a), which was consistent with the patterns of reduced tumor growth by TMZ (tumor growth inhibition 56.16%) and RG3039 (tumor growth inhibition 69.69%) at day 14 after tumor implantation (Fig. 4b–d). In the mice transplanted with U87 cells, RG3039 significantly prolonged the median OS from 17.5 days to 20 days (Fig. 4e). The growth of U87 cells was inhibited by RG3039 at day 10 after tumor implantation (Fig. 4f), with an approximate 50% decrease in average tumor volume (Fig. 4g–h). To evaluate any potential toxicity issue posed by RG3039, we administered RG3039 to healthy nude mice daily. After 40 days of administration, RG3039 did not impede the increase of mouse weight (Figure S4).

Taken together, these results indicated that RG3039 was well tolerated and had an anti-GBM activity comparable to that of TMZ in vivo.

The anti-GBM effect of DCPS inhibition was mediated by reducing STAT5B expression

To elucidate the mechanism of the anti-GBM effect of DCPS inhibition, we first examined the effects of RG3039 on the expression of previously identified target transcripts [21, 22]. We revealed that RG3039 significantly elevated the transcription levels of ATOH7 in U251 cells, as well as DRNT1 and DRNT2 in both U87 and U251 cells (Figure S5a–c). These results indicated that the effects of RG3039 on the expression of target transcripts in GBM cells were largely consistent with those reported in other cells, but still had their own characteristics.

Then, we treated four human GBM cell lines with RG3039 or DMSO and performed transcriptomic profiling by RNAseq. Transcription factor activity is commonly altered in cancer and frequently leads to sustained proliferative signaling, differentiation block and apoptosis resistance, all well-known hallmarks of cancer. Therefore, we focused on the effect of DCPS inhibition on the expressions of transcription factors [23]. The top 20 differentially expressed transcription factors were displayed in a heatmap and volcano plot (Fig. 5a–b). We focused on STAT5B, a member of the STAT family, because previous studies have shown that STAT5B works as a transcriptional activator in response to cytokines and growth factors during tumorigenesis and progression [24, 25].

To explore the role of STAT5B in mediating the anti-GBM effects of DCPS, we investigated the expression correlation between STAT5B and DCPS in TCGA GBM cohort by a linear regression model. DCPS expression and STAT5B expression were significantly positively correlated in TCGA GBM cohort, from the analysis of transcriptomic data ($R=0.42$; $p < 0.001$; Fig. 5c). Interference of DCPS expression genetically (by siRNA) or pharmacologically (by RG3039) significantly reduced the expression of STAT5B on both mRNA and protein levels in tumor cells (Fig. 5d–g).

To determine the role of STAT5B in the anti-GBM effects of DCPS inhibition, we overexpressed STAT5B in U87 and U251 cell lines through lentiviral infection. STAT5B overexpression decreased the sensitivity of tumor cells to RG3039, as indicated by the increase in the IC₅₀ of RG3039 in tumor cells (Fig. 6a). In apoptosis assays, the increased ratio of Annexin-V positive tumor cells induced by RG3039 was significantly lower upon

STAT5B overexpression, indicating that STAT5B overexpression inhibits the apoptosis of tumor cells treated with RG3039 (Fig. 6b, S6). The colony formation suppressed by RG3039 was rescued by STAT5B overexpression (Fig. 6c-d). Overall, our work shows that DCPS promotes the proliferation, survival and colony formation of GBM cells by regulating STAT5B expression (Fig. 6e).

Discussion

The role of DCPS in tumorigenesis and the anti-tumor efficacy of RG3039 have been reported in AML [10]. In the present study, we found that DCPS was overexpressed in GBM, and was related to more aggressive features of tumors and worse prognoses of patients with GBM. Using cell lines, GBOs, and an orthotopic GBM mouse model coupled with the bioinformatic analysis, we demonstrated the promising anti-GBM effect of DCPS inhibition, which may be mediated through downregulation of the expression of STAT5B.

Growing numbers of studies have uncovered that cancers are driven by alterations that affect each phase of RNA processing, including splicing, transport, editing and decay of messenger RNA [26, 27]. Thus, targeting mRNA processing has emerged as an attractive anti-cancer strategy [28, 29]. DCPS carries out the final step of the 3' to 5' end mRNA decay by clearing the cell of residual cap structure [4]. As the 5' cap structure and corresponding cap-binding proteins are integral components of various aspects of mRNA metabolism, including pre-mRNA splicing, nuclear export, translation, and decay, targeting DCPS may modulate cap structure accumulation and the pool of available cap-binding proteins in cells and in turn impact their downstream functions [4]. In the present study, we found that DCPS, a member of the histidine triad (HIT) superfamily, is abundantly expressed in GBM, and is increased compared with that in normal brain tissue [30]. In contrast, FHIT, another member of the HIT superfamily that has the function of clearing cap structure, is either absent or reduced in many types of tumors [30, 31]. This indicates that tumor cells might rely more heavily on DCPS to maintain the steady-state condition of cap degradation than normal cells, which may render them more vulnerable to DCPS inhibition. Consistent with this idea, Yamauchi et al. demonstrated that DCPS is essential for AML cell survival but is not necessary for steady-state hematopoiesis [10]. The DCPS inhibitor RG3039 has shown excellent central nervous system bioavailability in vivo [8, 9]. Importantly, a phase 1 clinical trial conducted by Repligen reported that RG3039 was safe and well tolerated by healthy volunteers.

To further confirm the anti-GBM efficacy of RG3039, we established GBOs derived from the freshly resected tumor tissues. Upon in vitro establishment and culture, GBOs demonstrate the structure and function of human

tumors to the greatest extent compared with cell lines and predict the therapeutic responses of patients. We first determined the fidelity of GBOs. The GBOs were stained with H&E and IHC, and an experienced neuro-oncologist confirmed that the GBOs had the pathological characteristics of the parental tumors. The molecular characteristics of GBOs and parental tumors were evaluated using WES, and the results showed that the GBOs retained approximately 70–80% of the gene mutations in the parental tumors, which was similar to the results reported in the literature [12]. The high intratumoral molecular heterogeneity of GBM [32–34] may account for the partial difference in molecular characteristics between GBOs and parental tumors. In the drug sensitivity assay, RG3039 had approximately the same IC_{50} as TMZ to GBOs, suggesting that the sensitivity of GBOs to RG3039 was similar to that of TMZ. This similarity was further verified using the orthotopic model of mouse GBM.

In the animal experiments, RG3039 was well tolerated; it significantly inhibited the growth of U251 cells and prolonged the survival of mice bearing U251 tumors. The median OS of mice in the control group, TMZ group, and RG3039 group were 23 days, 27 days and 29 days, respectively. The median OS of mice in the TMZ group was 4 days, approximately 17.4% longer than that in the control group. In patients with newly diagnosed GBM, adjuvant radiotherapy plus TMZ extended the median OS by approximately 20.7%, compared with that of patients receiving radiotherapy alone [35]. Therefore, the orthotopic model of mouse GBM used in this study reflects the clinical features of GBM, with rapid progression and poor therapeutic response. The dose of RG3039 used in the orthotopic model of mouse GBM was 20 mg/kg, which was tolerated and effective for SMA and AML mouse models [8, 10]. In the Guidance for Industry Estimating the Maximum Safe Starting Dose in Initial Clinical Trials for Therapeutics in Adult Healthy Volunteers issued by the FDA's Center for Drug Evaluation and Research in July 2005, the human equivalent dose of RG3039 20 mg/kg in mouse was approximately 1.6 mg/kg converted from body surface area. In the 2012 Annual SMA Conference, David Jacoby of Repligen reported that RG3039 at the highest dose tested (3 mg/kg) was safe and well tolerated in healthy volunteers enrolled in a phase 1 clinical trial of RG3039. In the present study, RG3039 effectively slowed the tumor growth in mice bearing orthotopic mouse GBM, but did not reduce the weight of healthy mice. These results suggest that the DCPS inhibitor RG3039, which has shown excellent central nervous system bioavailability in vivo and good tolerance in humans, exhibited robust anti-GBM activity in GBM cell lines, patient-derived organoids, and orthotopic mouse models, with drug exposure levels that are achievable in

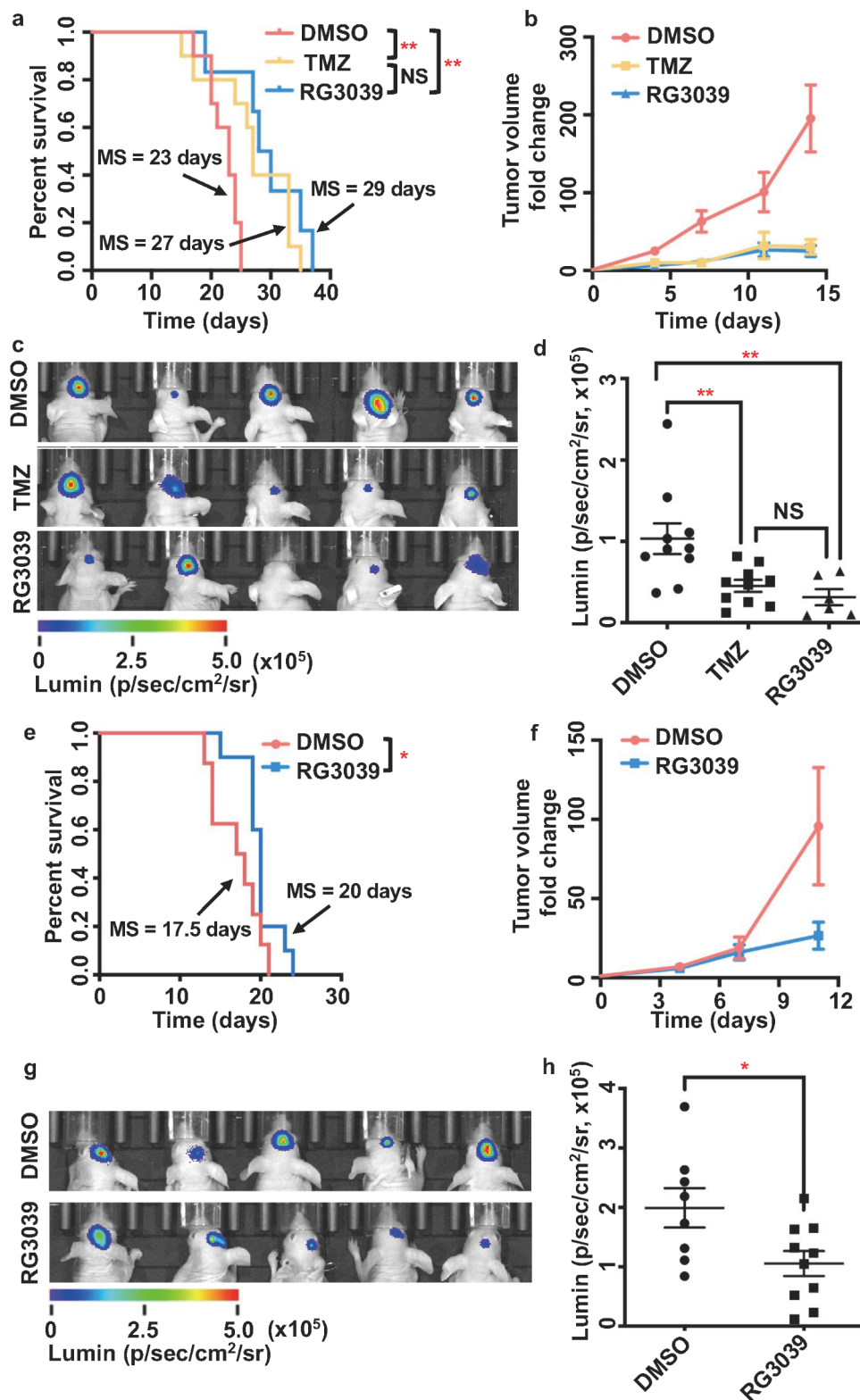


Fig. 4 (See legend on next page.)

(See figure on previous page.)

Fig. 4 The anti-GBM effect of RG3039 in orthotopic GBM mouse model

(a–d) GBM was induced by orthotopic implantation with U251 cells in BALB/c nude mice, and mice were treated with RG3039 ($n=6$), TMZ ($n=10$) or DMSO ($n=10$)

(a) Mouse survival was monitored and data were subjected to two-sided log-rank Mantel–Cox analysis ($n=6$ for RG3039 group, $n=10$ for TMZ group and $n=10$ for DMSO group). MS, median survival, NS, no significance, **, $p < 0.01$

(b) Fold change of tumor growth was analyzed by bioluminescence imaging 14 days after treatment (mean \pm SEM, $n=6$ for RG3039 group, $n=10$ for TMZ group and $n=10$ for DMSO group)

(c) Representative images of tumor volume measured by bioluminescence at day 14 after treatment

(d) Quantification of tumor volume measured by bioluminescence imaging at day 14 after treatment (mean \pm SEM, $n=6$ for RG3039 group, $n=10$ for TMZ group and $n=10$ for DMSO group). Statistical analysis by unpaired t-test, NS, no significance, **, $p < 0.01$

(e–h) GBM was induced by orthotopic implantation of U87 cells in BALB/c nude mice, and mice were treated with RG3039 ($n=10$) or DMSO ($n=8$)

(e) Mouse survival was monitored and data were subjected to two-sided log-rank Mantel–Cox analysis ($n=10$ for RG3039 group and $n=8$ for DMSO group). MS, median survival, NS, no significance, *, $p < 0.05$

(f) Fold change of tumor growth was analyzed by bioluminescence imaging 10 days after treatment (mean \pm SEM, $n=10$ for RG3039 group and $n=8$ for DMSO group)

(g) Representative images of tumor volume measured by bioluminescence at day 10 after treatment

(h) Quantification of tumor volume measured by bioluminescence imaging at day 10 after treatment (mean \pm SEM, $n=10$ for RG3039 group and $n=8$ for DMSO group). Statistical analysis by unpaired t-test, *, $p < 0.05$

humans. Our findings support the need for clinical trials to further evaluate the efficacy of RG3039 for patients with GBM as a novel therapy.

How DCPS inhibition suppresses proliferation and colonial formation and causes cellular apoptosis in GBM cells is not yet fully known. Our results suggest that reduction of STAT5B expression may partially account for the anti-GBM effects of DCPS inhibition. STAT5B has been implicated in development, progression, metastasis, survival and resistance of human cancers to treatment [24]. STAT5B exhibits oncogenic activity through transcriptional alterations or protein-protein interactions, regulating the *TGF- β* , *PI3K/PTEN* and *HIF1 α* signaling pathways, anti-apoptotic pathways via down-regulation of miRNA15/16 and up-regulation of Bcl-2, MCL-1 and Bcl-XL, the G1/S transition via up-regulation of cyclin D1, D2, D3 and c-Myc and the DNA damage control pathway via up-regulation of RAD51 [24, 36]. How DCPS inhibition precisely downregulates STAT5B expression is unknown. The degradation of cap structures is the intrinsic function of DCPS, which would consequently modulate the pool of available cap-binding proteins in a cell. DCPS may regulate the cap-proximal pre-mRNA splicing, mRNA transport and mRNA translation [4]. It is intriguing to postulate that various aspects of STAT5B mRNA metabolism may be modulated by DCPS inhibition. Further investigation is needed to elucidate therapeutic mechanisms of DCPS inhibition.

Conclusions

In summary, we demonstrated that DCPS was overexpressed in GBM and that DCPS may be a novel therapeutic target for GBM. The DCPS inhibitor RG3039 exhibited robust anti-GBM activity, with drug exposures achievable in humans. The anti-GBM effect of DCPS inhibition was potentially mediated through the reduction in STAT5B expression. Our findings warrant clinical

trials to evaluate the efficacy of RG3039 as a novel therapy for patients with GBM.

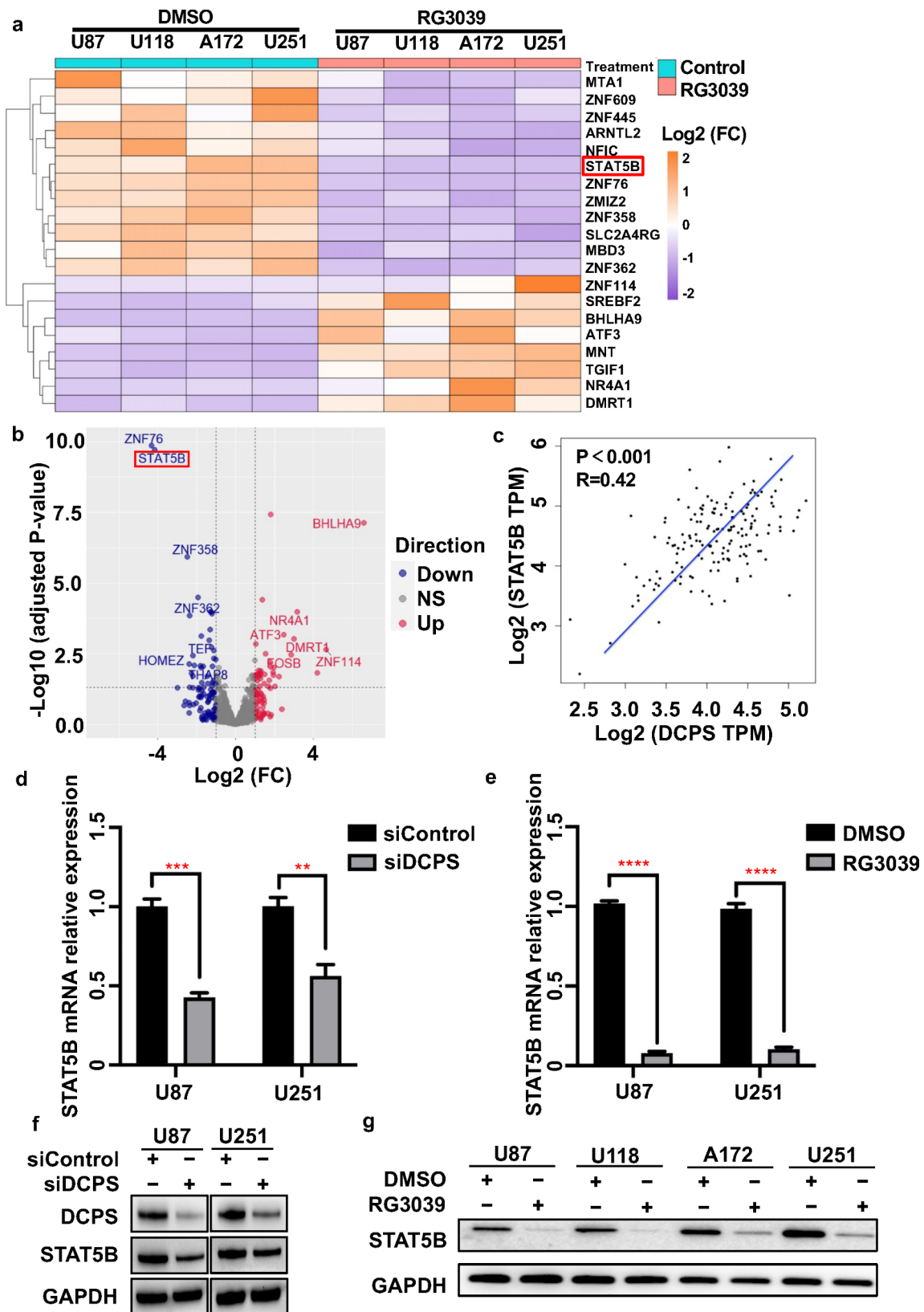


Fig. 5 (See legend on next page.)

(See figure on previous page.)

Fig. 5 DCPS inhibition reduced STAT5B expression in GBM cells

(a–b) GBM cell lines were treated with RG3039 (6 μ M) or DMSO for 48 h and then subjected to RNAseq. The top 20 differentially expressed transcription factors were displayed in heatmap **(a)** and volcano plot **(b)**. FC, fold change

(c) Correlation analysis of the expressions of DCPS and STAT5B in GBMs in TCGA database. Statistical analysis by linear regression analysis

(d) GBM cell lines were transfected with siRNA targeting DCPS for 48 h. The expression of STAT5B mRNA was analyzed by RT-qPCR and normalized to that of β -actin (mean \pm SEM, $n=3$). Statistical analysis by unpaired t-test, **, $p < 0.01$, ***, $p < 0.001$

(e) GBM cell lines were treated with RG3039 (6 μ M) or DMSO for 48 h. The expression of STAT5B mRNA was analyzed by RT-qPCR and normalized to that of β -actin (mean \pm SEM, $n=3$). Statistical analysis by unpaired t-test, ****, $p < 0.0001$

(f) GBM cell lines were transfected with siRNA targeting DCPS for 48 h. The expressions of DCPS and STAT5B were analyzed by western blotting

(g) GBM cell lines were treated with RG3039 (6 μ M) or DMSO for 48 h. The expression of STAT5B was analyzed by western blotting

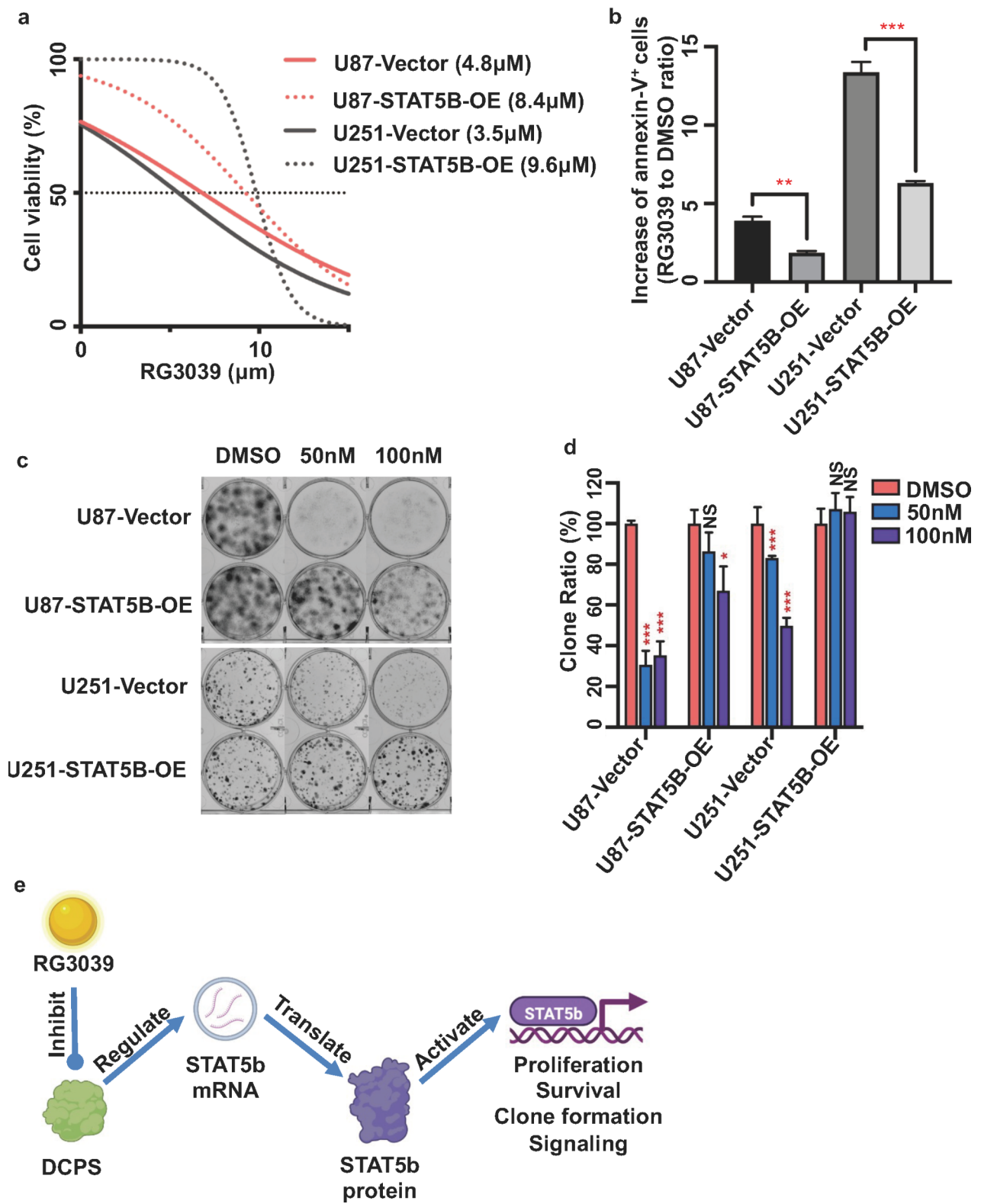


Fig. 6 (See legend on next page.)

(See figure on previous page.)

Fig. 6 The anti-GBM effect of DCPS inhibition was mediated through reducing STAT5B expression

(a) GBM cell lines with STAT5B overexpression or vector expression were treated with various concentrations of RG3039 or DMSO for 72 h. The IC50 of RG3039 was analyzed by CCK-8 assay ($n = 3$)

(b) Quantification of the ratio of Annexin-V-positive cells in apoptosis assays (see Figure S2b for details) in GBM cell lines with STAT5B overexpression or vector expression treated with RG3039 (6 μ M) to that of cells treated with DMSO (mean \pm SEM, $n = 3$). Statistical analysis by unpaired t-test, **, $p < 0.01$, ***, $p < 0.001$

(c) Representative images of colony formation assays in GBM cell lines with STAT5B overexpression or vector expression treated with various concentrations of RG3039 or DMSO for 14 days

(d) Quantification of the ratio of colony formation of GBM cells with STAT5B overexpression or vector treated with RG3039 to cells treated with DMSO (mean \pm SEM, $n = 3$). Statistical analysis by unpaired t-test, NS, no significance, *, $p < 0.05$, ***, $p < 0.001$

(e) Schematic diagram summarizing that RG3039 inhibits DCPS regulating the expression of STAT5B, which plays an essential role in tumor progression

Abbreviations

GBM	Glioblastoma
DCPS	mRNA decapping enzyme scavenger
STAT5B	Signal transducer and activator of transcription 5B
CNS	Central nervous system
OS	Overall survival
SMA	Spinal muscular atrophy
AML	Acute myeloid leukemia
GBOs	Glioblastoma organoids
FFPE	Formalin fixed paraffin-embedded
KPS	Karnofsky performance status
SVZ	Subventricular zone
EOR	Extent of resection
IDH-1	Isocitrate dehydrogenase 1
MGMT	O6-DNA-methylguanine methyltransferase
MRI	Magnetic resonance imaging
GTR	Gross total resection
STR	Subtotal resection
TCGA	The Cancer Genome Atlas
CGGA	Chinese Glioma Genome Atlas
TMZ	Temozolomide
IHC	Immunohistochemistry
DAB	3,3-diaminobenzidine
HPFs	High-power fields
WES	Whole exome sequencing
CNVs	Copy number variations
HIT	Histidine triad

Foundation (2020A1515110069), the Natural Science Foundation of Sichuan Province (2023NSFSC1884), and the Postdoctor Research Fund of West China Hospital, Sichuan University (2023HXBH105).

Data availability

The data and materials for this research are available from the corresponding author on reasonable request.

Declarations

Ethics approval and consent to participate

The Medical Ethics Committees of Sun Yat-sen University Cancer Center approved this study (no. B2021-427-01). All procedures performed in this study involving human participants were in accordance with the ethical standards of the Medical Ethics Committees of Sun Yat-sen University Cancer Center, followed the 1964 Helsinki Declaration and its later amendments. Informed consent to review medical data was obtained from all patients.

Consent for publication

Not applicable.

Conflict of interest

K.T. Flaherty reports personal fees and other support from Clovis Oncology, Kinnate Biopharma, Checkmate Pharmaceuticals, Strata Oncology, Scorpion Therapeutics, PIC Therapeutics, Apricity, Tvardi, xCures, Monopteros, Vibliome, ALX Oncology, Fog Pharma, and Soley Therapeutics, as well as personal fees from Nextech, Takeda, Transcode Therapeutics, and Novartis during the conduct of the study. No disclosure is reported by the other authors.

Author details

¹Department of Neurosurgery/Neuro-Oncology, State Key Laboratory of Oncology in South China, Guangdong Provincial Clinical Research Center for Cancer, Sun Yat-sen University Cancer Center, Guangzhou, China

²Department of Thoracic Surgery, State Key Laboratory of Oncology in South China, Guangdong Provincial Clinical Research Center for Cancer, Sun Yat-sen University Cancer Center, Guangzhou, China

³Experimental Animal Center, The First Affiliated Hospital of Sun Yat-sen University, Guangzhou, China

⁴Department of Thoracic Surgery, Institute of Thoracic Oncology, West China Hospital, Sichuan University, Chengdu 610041, China

⁵Department of Pathology, State Key Laboratory of Oncology in South China, Guangdong Provincial Clinical Research Center for Cancer, Sun Yat-sen University Cancer Center, Guangzhou, China

⁶Department of Medical Oncology, State Key Laboratory of Oncology in South China, Guangdong Provincial Clinical Research Center for Cancer, Sun Yat-sen University Cancer Center, Guangzhou, China

⁷Guangdong Research Center of Organoid Engineering and Technology, Guangzhou, China

⁸Faculty of Dentistry, University of Hong Kong, Hong Kong Special Administrative Region, Hong Kong, China

⁹Department of Medicine, Massachusetts General Hospital, Massachusetts General Hospital Cancer Center, Harvard Medical School, Boston, MA, USA

¹⁰Department of Statistics, Rutgers University, New Brunswick, NJ, USA

¹¹Ovarian Cancer Research Center, Division of Gynecologic Oncology, Department of Obstetrics & Gynecology, Perelman School of Medicine, University of Pennsylvania, Philadelphia, PA, USA

Supplementary Information

The online version contains supplementary material available at <https://doi.org/10.1186/s12967-024-05658-x>.

Supplementary Material 1

Supplementary Material 2

Acknowledgements

We thank Accurate International Biotechnology Co. for their assistance with the organoid techniques, and Gabrielle White Wolf, PhD, from Liwen Bianji (Edanz) (www.liwenbianji.cn) for editing the English text of a draft of this manuscript.

Author contributions

All authors made substantial contributions to the conception or design of the study; the acquisition analysis, or interpretation of data; or drafting or revising the manuscript. All authors approved the manuscript. HD, G.Zhang, KTF, HX, WM and YM designed the study and analyses. HD, WH, YY and YM provided tumor specimens. Experiments were performed by HD, YX, SW, G.Zhao, HH, YY, ZC, WM, and ZZ. Data analysis was performed by HD, YX, SW, G.Zhao, WH, YC, SH, HX, WM and YM. The manuscript and figures were prepared by HD, YX, HX, WM and ZZ with input from all authors. The manuscript was revised by HD, YX and ZZ. The study was supervised by YM, WM and HX.

Funding

This work was supported by the National Natural Science Foundation of China (82002628, 82303805), the Guangdong Basic and Applied Basic Research

¹²Intensive Care Unit, State Key Laboratory of Oncology in South China, Guangdong Provincial Clinical Research Center for Cancer, Sun Yat-sen University Cancer Center, Guangzhou, China

Received: 14 April 2024 / Accepted: 4 September 2024

Published online: 30 September 2024

References

- Ostrom QT, et al. CBTRUS statistical report: primary brain and central nervous system tumors diagnosed in the United States in 2006–2010. *Neuro Oncol*. 2013;15(Suppl 2):ii1–56.
- Stupp R, et al. Effect of Tumor-Treating Fields Plus maintenance temozolomide vs maintenance temozolomide alone on survival in patients with glioblastoma: a Randomized Clinical Trial. *JAMA*. 2017;318(23):2306–16.
- Tourriere H, Chebli K, Tazi J. mRNA degradation machines in eukaryotic cells. *Biochimie*. 2002;84(8):821–37.
- Bail S, Kiledjian M. DcpS, a general modulator of cap-binding protein-dependent processes? *RNA Biol*. 2008;5(4):216–9.
- Jiao X, et al. A mammalian pre-mRNA 5' end capping quality control mechanism and an unexpected link of capping to pre-mRNA processing. *Mol Cell*. 2013;50(1):104–15.
- Wang ZR, Kiledjian M. Functional link between the mammalian exosome and mRNA decapping. *Cell*. 2001;107(6):751–62.
- van Dijk E, Le Hir H, Seraphin B. DcpS can act in the 5'-3' mRNA decay pathway in addition to the 3'-5' pathway. *Proc Natl Acad Sci USA*. 2003;100(21):12081–6.
- Gogliotti RG, et al. The DcpS inhibitor RG3039 improves survival, function and motor unit pathologies in two SMA mouse models. *Hum Mol Genet*. 2013;22(20):4084–101.
- Van Meerbeke JP, et al. The DcpS inhibitor RG3039 improves motor function in SMA mice. *Hum Mol Genet*. 2013;22(20):4074–83.
- Yamauchi T, et al. Genome-wide CRISPR-Cas9 screen identifies leukemia-specific dependence on a Pre-mRNA metabolic pathway regulated by DCP5. *Cancer Cell*. 2018;33(3):386–e4005.
- Lim DA, et al. Relationship of glioblastoma multiforme to neural stem cell regions predicts invasive and multifocal tumor phenotype. *Neuro Oncol*. 2007;9(4):424–9.
- Jacob F, et al. A patient-derived Glioblastoma Organoid Model and Biobank recapitulates Inter- and intra-tumoral heterogeneity. *Cell*. 2020;180(1):188–e20422.
- Ma W, et al. High expression of Indoleamine 2, 3-Dioxygenase in Adenosquamous Lung Carcinoma Correlates with favorable patient outcome. *J Cancer*. 2019;10(1):267–76.
- Duan H, et al. KIF-2 C expression is correlated with poor prognosis of operable esophageal squamous cell carcinoma male patients. *Oncotarget*. 2016;7(49):80493–507.
- Bolger AM, Lohse M, Usadel B. Trimmomatic: a flexible trimmer for Illumina sequence data. *Bioinformatics*. 2014;30(15):2114–20.
- Li H. *Aligning sequence reads, clone sequences and assembly contigs with BWA-MEM*. arXiv preprint arXiv:1303.3997, 2013.
- Van der Auwera GA, et al. From FastQ data to high confidence variant calls: the Genome Analysis Toolkit best practices pipeline. *Curr Protoc Bioinf*. 2013;43(1110):11101–111033.
- McKenna A, et al. The genome analysis Toolkit: a MapReduce framework for analyzing next-generation DNA sequencing data. *Genome Res*. 2010;20(9):1297–303.
- Cibulskis K, et al. Sensitive detection of somatic point mutations in impure and heterogeneous cancer samples. *Nat Biotechnol*. 2013;31(3):213–9.
- Sun A et al. *Firefly luciferase-based dynamic bioluminescence imaging: a noninvasive technique to assess tumor angiogenesis*. *Neurosurgery*, 2010. 66(4): pp. 751-7; discussion 757.
- Zhou M, et al. DcpS is a transcript-specific modulator of RNA in mammalian cells. *RNA*. 2015;21(7):1306–12.
- Gentillon C, et al. The effects of C5-substituted 2,4-diaminoquinazolines on selected transcript expression in spinal muscular atrophy cells. *PLoS ONE*. 2017;12(6):e0180657.
- Bushweller JH. Targeting transcription factors in cancer - from undruggable to reality. *Nat Rev Cancer*. 2019;19(11):611–24.
- Yu H, Jove R. The STATs of cancer—new molecular targets come of age. *Nat Rev Cancer*. 2004;4(2):97–105.
- Furqan M, et al. STAT inhibitors for cancer therapy. *J Hematol Oncol*. 2013;6:90.
- Obeng EA, Stewart C, Abdel-Wahab O. Altered RNA Processing in Cancer Pathogenesis and Therapy. *Cancer Discov*. 2019;9(11):1493–510.
- Tan K, Stupack DG, Wilkinson MF. Nonsense-mediated RNA decay: an emerging modulator of malignancy. *Nat Rev Cancer*. 2022;22(8):437–51.
- Desterro J, Bak-Gordon P, Carmo-Fonseca M. Targeting mRNA processing as an anticancer strategy. *Nat Rev Drug Discov*. 2020;19(2):112–29.
- Lindeboom RGH, et al. The impact of nonsense-mediated mRNA decay on genetic disease, gene editing and cancer immunotherapy. *Nat Genet*. 2019;51(11):1645–51.
- Martin J, St-Pierre MV, Dufour JF. Hit proteins, mitochondria and cancer. *Biochim Biophys Acta*. 2011;1807(6):626–32.
- Silveira Zavalhia L, et al. Do FHIT gene alterations play a role in human solid tumors? *Asia Pac J Clin Oncol*. 2018;14(5):e214–23.
- Neftel C, et al. An Integrative Model of Cellular States, plasticity, and Genetics for Glioblastoma. *Cell*. 2019;178(4):835–e84921.
- Darmanis S, et al. Single-cell RNA-Seq analysis of infiltrating neoplastic cells at the Migrating Front of Human Glioblastoma. *Cell Rep*. 2017;21(5):1399–410.
- Patel AP, et al. Single-cell RNA-seq highlights intratumoral heterogeneity in primary glioblastoma. *Science*. 2014;344(6190):1396–401.
- Stupp R, et al. Radiotherapy plus concomitant and adjuvant temozolomide for glioblastoma. *N Engl J Med*. 2005;352(10):987–96.
- Paukku K, Silvennoinen O. STATs as critical mediators of signal transduction and transcription: lessons learned from STAT5. *Cytokine Growth Factor Rev*. 2004;15(6):435–55.

Publisher's note

Springer Nature remains neutral with regard to jurisdictional claims in published maps and institutional affiliations.